Solvent relaxation effects on the kinetics of photoinduced electron transfer reactions

J. Najbar,[a] R. C. Dorfman, and M. D. Fayer
Department of Chemistry, Stanford University, Stanford, California 94305

(Received 18 September 1990; accepted 12 October 1990)

The three-potential surface problem of electron transfer in solution is analyzed using Zusman-type kinetic equations. The model describes ultrafast formation and recombination of radical–ion pairs limited by solvent dielectric relaxation. The problem begins with a donor on an electronic excited state surface. The system evolves with crossing to the radical–ion pair surface (with the possibility of recrossing to the excited donor surface included). Solvent relaxation moves the system to lower energy on the radical–ion pair surface where crossing to the ground state neutral surface occurs (with the possibility of recrossing to the radical–ion surface included). Model calculations of the transient radical–ion pair populations are presented. The time dependent results that are presented show a dramatic dependence on the relative free energy differences (ΔG's) among the three potential surfaces. Comparisons to other formalisms and to less detailed approximations are made. The mean populations of the transient species for a system of a donor and many acceptors in the absence of spatial diffusion are also derived.

I. INTRODUCTION

The kinetics of the transient species (radical–ions, excited states) created in photoinduced electron transfer reactions has attracted the attention of many research groups working in the fields of chemistry, photophysics of radicals, spin dynamics, and the physics of charge separation.[1–4] The understanding of these electron transfer processes expanded during the 1980's due to the development of new ultrafast laser spectroscopic techniques and new theoretical procedures for reaction dynamics in the liquid state.[5–12] In this paper, a straightforward model is used to describe the motion on the polarization coordinate (distribution function) of the transient species produced in an electron transfer reaction. The distribution function is then used to calculate the populations of the transient species. These can be related to experimental observables. The calculations are peformed in Laplace space and the final results are back transformed to the time domain.

The first theories describing electron transfer in polar solvents were classical in nature. Early Marcus theory,[2] was formulated in terms of transition state theory. The results gave rate constants in terms of the static dielectric properties of the solvent.[13,14] More recently, quantum-mechanical theories were used to derive the rate constants for nonadiabatic electron transfer reactions. These rate constants were written in the form of the Fermi golden rule. The rate depended on the Franck–Condon factors for the nuclear degrees of freedom of the reactants and the solvent.[15,16] A comparison of the classical and the more recent quantum-mechanical theories was an important step in understanding ultrafast reactions in solution. The limitations of transition state theory and the role of coupling between the reaction coordinate and solvent degrees of freedom were evaluated.[14,17–22] This helped to distinguish different reaction regimes and led to the concept of frequency dependent friction on the molecular level.[18–20] The development of the idea of friction on the molecular level has occured in fields of the theory of stochastic processes,[11,12] theory of dipolar liquids and solvation[10,22] and in molecular dynamics simulations.[23,24]

The interaction energy of charged species with polar solvents is comparable with chemical binding energies. For this reason, the dynamics of solvation plays a role in charge–transfer reactions. A one-dimensional reaction coordinate is used to describe electron transfer reactions in solution. This coordinate describes the polarization fluctuations of the solvent induced by charged species. An important element of Marcus' theory is that the response of the environment to a charge is approximately linear. Thus, the free energy of the system can be approximated by a quadratic function of the polarization coordinate. A reaction diagram connecting the reactant and product states can be represented by two intersecting parabolas (see Fig. 1). A consequence of the quadratic dependence of the free energy on the polarization coordinate is the existence of the normal and inverted regions. In the normal free energy region the reaction rate increases with increasing exothermicity. The reaction rate decreases with increasing exothermicity in the inverted region.

The interaction of charged species with solvent is long range. Continuum theories of solvation dynamics predict that the solvent polarization equilibrates on the time scale of the longitudinal dielectric relaxation time $\tau_L = \tau_D \epsilon_\infty / \epsilon_0$, where τ_D is the Debye dielectric relaxation time, ϵ_∞ and ϵ_0 are the optical and static dielectric constants. Experimental verification of the existence of the Marcus inverted region[25] and the importance of the time scale of the longitudinal dielectric relaxation[26] have had a large impact on current interest in electron transfer reactions and recent theoretical developments, particularly in the development of microscopic theories. This development was also facilitated by large-scale computer simulations (molecular dynamics) of

[a] On leave from: Jagiellonian University, Faculty of Chemistry, 30-060 Krakow, Poland.

 0021-9606/91/021081-12$03.00

dipolar liquids.[23,24] Application of the mean spherical approximation[28,29] and relating the solvent polarization correlation function to the macroscopic frequency dependent dielectric function $\epsilon(\omega)$[10,30–34] were important steps in the development of microscopic theories. Further development showed that the dynamics of solvation is related to the frequency and wave vector dependent dielectric function $\epsilon(\mathbf{k},\omega)$.[30–39] It was discovered that not only rotational motions of polar solvent molecules are involved in the dynamics, but also translational motions of solvent molecules may influence dielectric polarization relaxation around charged species.[30–33]

Recently, Mukamel and co-workers[12,34–39] have shown the connection between outer-sphere solvent controlled electron transfer processes and third-order nonlinear spectroscopy and the theory of optical line shapes. Liouville space generating function methods and four-point correlation functions were employed to describe the dynamics of the polarization coordinate.[12,34–36] Their approach is more general than previous theories in relation to the problem of time scale separation of coherence and that of population decay, and is not limited to the static Gaussian equilibrium distribution of the reaction coordinate.

Different theoretical techniques were employed to solve the problem of a two-level system interacting with the solvent (bath). The general approach is based on the stochastic Liouville equation for the density matrix. Important results have been obtained by Onuchic and co-workers using path integral methods.[41–46] They have been able to include the effects of internal reorganization energy, and derive the corresponding Fokker–Planck stochastic equations. The methods using the Liouville space generating functions are suitable for the evaluation of four-point correlation functions popular in the theory of nonlinear optical phenomena (CARS, transient grating, four-wave mixing, hole burning).[12,40] The analogy between outer-sphere electron transfer and nonlinear optics is especially interesting since various stochastic and microscopic models were developed using four-point correlation functions.

As mentioned above there are several reaction regimes. The electron transfer process may occur nonadiabatically or adiabatically when the electronic interactions are large and solvent relaxation is relatively slow. The transition between these two reaction regimes can be described in terms of Smoluchowski-type kinetic equations derived from the Liouville equation for the density matrix of a two-level system. These equations were derived by Zusman[47,48] and rederived by Onuchic.[41,43] The solution of the equations were given by Zusman[47,48] and Rips and Jortner.[49,50] Recently, the solutions of these equations were investigated and compared with computer simulations based on the generalized Langevin equation by Fonseca.[51] The theory gives the expressions for the rate coefficients in the long time approximation and allows for the description of the transient effects at short times.

The transient species formed due to photoinduced electron transfer can be described in terms of a two-potential surface system if the back electron transfer reaction leading to ground state recovery is slow. For the analysis of ultrafast forward and reverse electron transfer reactions a three-surface model is more appropriate. On the time scale of interest (picoseconds or femtoseconds) spin dynamics is rather slow. The rates of interconversion of the spin states (singlet and triplet states of the radical–ion pairs) are of order 0.1 ns^{-1}. On the time scale of picoseconds we can neglect the interconversion between these states and limit our attention to the state of the radical pair of the same multiplicity as the multiplicity of the initial state from which the radical–ion pair was created.

Here we are interested in the case where the back electron transfer step leading to ground state recovery occurs on the same time scale as solvent dielectric relaxation. For this reason the kinetic problem cannot be easily divided into two separate two-surface problems. After the forward electron transfer step, the recombination process occurs before the transient radical pair is equilibrated with the solvent degrees of freedom. In this paper we propose an extension of the kinetic equations, derived by Zusman[47,48] and Onuchic,[43] to treat the three-surface problem.

The limitation of the proposed approach is that it neglects the effects connected with the internal degrees of freedom of the reactants (e.g., internal reorganization energy) for the electron transfer processes. It is possible to include the effects of the internal degrees of freedom in a manner similar to Sumi and Marcus.[55] This is discussed further below.

The utility of the kinetic equations applied here are that they are simple enough for numerical analysis and detailed information concerning the solvent relaxation dynamics can be incorporated into this model. The solvent relaxation properties are incorporated via an autocorrelation function of the solvent polarization coordinate. Thus, non-Debye dielectric solvent relaxation can be taken into account.

Solvent dynamics influence the electron transfer rates at short and long time scales. At $t = 0$ the initial excited state has a nonequilibrium value in the solvent polarization coordinate. In a time-resolved experiment of the fluorescence band shift, time evolution of the initial nonequilibrium distribution in the polarization coordinate is monitored.[27] Under such conditions, the influence of solvent dynamics on the reaction rates is predominant. The results obtained here clearly illustrate the role that the dynamics of solvent relaxation has on charge generation and charge recombination. It is found that the dynamics depend very strongly on the relative positions (ΔG's) of the three-potential surfaces. This is reflected in the time-dependent radical–ion populations. In addition, monitoring the population of radical–ion pairs formed by photoinduced electron transfer reactions can permit investigation of the solvent dielectric relaxation.

In Sec. II the formal mathematical development is presented. In Sec. III numerical calculations are given, for particular parameters, of the time dependencies of the important quantities that appear in the theory. These include the radical–ion pair populations as a function of ΔG and the solvent relaxation rate. Concluding remarks are given in Sec. IV. In Appendix A the relationship between this theory and simple approaches that use transfer rate constants is considered and in Appendix B, the theory is formally generalized to a distribution of donor–acceptor distances.

II. TRANSIENT POPULATION OF THE RADICAL-ION PAIRS

Consider an excited electron donor/acceptor or an electron acceptor/donor quencher separated by fixed distance in a polar solvent. Electron transfer between donor and acceptor produces radical–ion pairs. Back electron transfer deactivates the system to the ground state. This is shown in Fig. 1. Usually treated separately from the electron transfer processes, the initial state e can directly relax to the ground state g due to radiative and radiationless transitions with the rate constant $1/\tau$. We assume that the lifetime of the excited molecule in the absence of quencher is much larger than the solvent relaxation time.

In terms of the polarization coordinate q, the free energy profiles $G_x(q)$ for the system are composed of three harmonic wells, one centered at $q=0$ corresponding to the reactants, the second at $q=q_1$ for the radical pair, and the third centered at $q=q_2=0$, which is the ground state. The corresponding potential functions are given by

$$G_e(q) = \tfrac{1}{2}kq^2, \tag{1a}$$

$$G_r(q) = \tfrac{1}{2}k(q-q_1)^2 + \Delta G_r, \tag{1b}$$

$$G_g(q) = \tfrac{1}{2}k(q-q_2)^2 + \Delta G_g, \tag{1c}$$

where $G_g(q)$, $G_e(q)$, and $G_r(q)$ are the ground, excited (initial), and radical–ion states respectively. ΔG_r and ΔG_g are the zero-point free energies of the radical and ground states, respectively, with the zero of energy taken at the bottom of the G_e surface (see Fig. 1).

The force constant $k=1/2\lambda$ is assumed to be common for these three wells. This is the simplest case. It is possible to extend this model to different force constants for each surface but this would double the number of crossing points and make the calculations more complex without gaining new physical information. λ is the solvent reorganization energy. Consider two crossing points, c_1 between G_e and G_r diabatic surfaces and c_2 between G_r and G_g [illustrated in Fig. 1 for $G_r(q)$ curve A]. The crossing points c_1 and c_2 can be found from the equations $G_e(q)=G_r(q)$ and $G_r(q)=G_g(q)$, respectively:

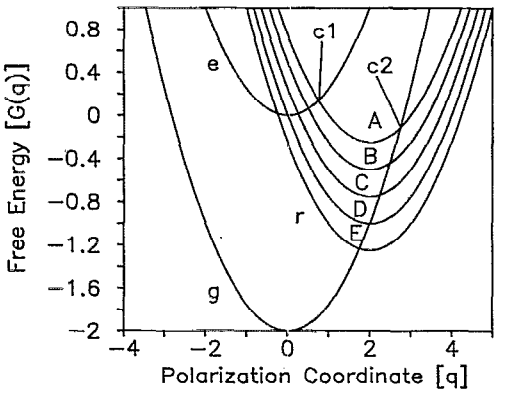

FIG. 1. The free-energy functions $G(q)$ for the forward and back outer-sphere electron transfer reactions in polar solvent. The parameters used to generate this plot are the same as used in Figs. 2–6.

$$c_1 = \frac{1}{2}q_1 + \frac{\Delta G_r}{kq_1}, \tag{2}$$

$$c_2 = \frac{1}{2}(q_1+q_2) + \frac{(\Delta G_g - \Delta G_r)}{k(q_1-q_2)}. \tag{3}$$

There is no crossing point between the G_e and G_g potential functions.

The dynamics on each potential surface can be described in terms of the Green function $\phi(q,q',t)$ of the following equation[49–51]:

$$\left(\frac{\partial}{\partial t} - L_{\text{eff}}\right)\phi(q,q',t) = 0 \tag{4}$$

with initial condition $\phi(q,q',0)=\delta(q-q')$. L_{eff} is the effective Liouvillian operator for the reaction coordinate. We use the solution of the equation for the harmonic system in the overdamped limit. The Green function is given in terms of the time correlation function of the reaction coordinate[21,22,47,48,51]

$$\Delta(t) = \frac{\langle \delta q(0)\delta q(t)\rangle}{\langle \delta q(0)^2\rangle} \tag{5}$$

by the following equation:

$$\phi(q,q',t) = \exp\left(-\frac{[q-q'\Delta(t)]^2}{2\langle q^2\rangle[1-\Delta(t)^2]}\right)\Big/ \sqrt{2\pi\langle q^2\rangle[1-\Delta(t)^2]}, \tag{6}$$

where $\langle q^2\rangle = 2\lambda k_b T$ (k_b is Boltzmann's constant). For a Debye solvent $\Delta(t)=\exp(-t/\tau_L)$, where τ_L is the longitudinal relaxation time of the solvent. Equation (6) gives the conditional probability for the reaction coordinate to have value q at time t, given that it had value q' at $t=0$ and that system is on a single-potential surface. In a more general theory presented by Mukamel and co-workers,[12,34–39] four-point time correlation functions are used to describe the time evolution of the distribution function of the reaction coordinate.

Let us define $\rho_e(q,t)$,$\rho_r(q,t)$, and $\rho_g(q,t)$ as the probability distribution functions for the reaction coordinate q at time t belonging to the reactants e, radical–ion pair r, and the ground state g wells, respectively. For the three-surface system we apply the following kinetic equations:

$$\frac{\partial \rho_e(q,t)}{\partial t} = -H_{er}(q,t)\delta(q-c_1) + L_{\text{eff}}\rho_e(q,t), \tag{7a}$$

$$\frac{\partial \rho_r(q,t)}{\partial t} = H_{er}(q,t)\delta(q-c_1) - H_{rg}(q,t)\delta(q-c_2) + L_{\text{eff}}\rho_r(q,t), \tag{7b}$$

$$\frac{\partial \rho_g(q,t)}{\partial t} = +H_{rg}(q,t)\delta(q-c_2) + L_{\text{eff}}\rho_g(q,t). \tag{7c}$$

$H_{er}(q,t)$ and $H_{rg}(q,t)$ represent the electronic coupling between pairs of the diabatic surfaces $s-r$ and $r-g$, respectively. They are given by

$$H_{er}(q,t) = \frac{2\pi V_{er}^2}{\hbar}[\rho_e(q,t) - \rho_r(q,t)], \tag{8}$$

$$H_{rg}(q,t) = \frac{2\pi V_{rg}^2}{\hbar}[\rho_r(q,t) - \rho_g(q,t)], \tag{9}$$

where V_{er} and V_{rg} are electronic coupling matrix elements between $s-r$ and $r-g$ diabatic surfaces, respectively. Equations (8) and (9) assume that the couplings are only effective at the crossing points c_1 and c_2 of the corresponding potential functions. This means that transfer from one surface to another will occur only at that level of solvent relaxation. In other words, there is a narrow range of configurations that are appropriate transition states between the surfaces. The dynamics of the polarization coordinate within each potential well is governed by a common effective Liouvillian operator $L_{\rm eff}$ because the potential functions are identical. This operator governs the motion of the radical–ion pairs as they travel on the potential surfaces. This accounts for the thermodynamic tendency for the system to relax to a lower energy state (relaxed solvent) and for thermal fluctuations accounting for the finite distribution of radical–ion pairs over different states of solvent relaxation. The different surfaces are only shifted in energy scale and the reaction coordinate. The energy scale difference accounts for the changes in electronic energy between the ground, excited and radical–ion states. The reaction coordinate shows how the solvent must change as the electron transfer and back transfer proceed.

The Laplace transformation of Eqs. (7a)–(7c) gives

$$s\bar{\rho}_e(q,s)-\rho_e(q,t=0)=-\bar{H}_{er}(q,s)\delta(q-c_1)+L_{\rm eff}\bar{\rho}_e(q,s), \tag{10a}$$

$$s\bar{\rho}_r(q,s)=\bar{H}_{er}(q,s)\delta(q-c_1)-\bar{H}_{rg}(q,s)\delta(q-c_2)+L_{\rm eff}\bar{\rho}_r(q,s), \tag{10b}$$

$$s\bar{\rho}_g(q,s)=\bar{H}_{rg}(q,s)\delta(q-c_2)+L_{\rm eff}\bar{\rho}_g(q,s), \tag{10c}$$

where we assumed $\rho_e(q,t=0)=1$, $\rho_g(q,t=0)=0$, and $\rho_r(q,t=0)=0$ since at $t=0$ there is no population of other species except in the initial level. The Laplace transformation of Eq. (4) gives

$$(s-L_{\rm eff})\bar{\phi}(q,q',s)=\delta(q-q'). \tag{11}$$

The solution of the Laplace transformed kinetic equations (10a)–(10c) are given in terms of the Laplace transform of the Green function:

$$\bar{\rho}_e(q,s)=-\bar{H}_{er}(c_1,s)\bar{\phi}(q,c_1,s)+\int_{-\infty}^{\infty}\bar{\phi}(q,q',s)\rho_e(q',t=0)dq', \tag{12a}$$

$$\bar{\rho}_r(q,s)=\bar{H}_{er}(c_1,s)\bar{\phi}(q-q_1,c_1-q_1,s)-\bar{H}_{rg}(c_2,s)\bar{\phi}(q-q_1,c_2-q_1,s), \tag{12b}$$

$$\bar{\rho}_g(q,s)=\bar{H}_{rg}(c_2,s)\bar{\phi}(q,c_2,s), \tag{12c}$$

where

$$\bar{H}_{er}(c_1,s)=\frac{2\pi V_{er}^2}{\hbar}[\bar{\rho}_e(c_1,s)-\bar{\rho}_r(c_1,s)], \tag{13}$$

$$\bar{H}_{rg}(c_2,s)=\frac{2\pi V_{rg}^2}{\hbar}[\bar{\rho}_r(c_2,s)-\bar{\rho}_g(c_2,s)]. \tag{14}$$

Solving Eqs. (12)–(14) for $\bar{H}_{er}(c_1,s)$ and $\bar{H}_{rg}(c_2,s)$ we obtain

$$\bar{H}_{er}(c_1,s)=\frac{2\pi V_{er}^2}{\hbar}\int_{-\infty}^{\infty}\bar{\phi}(c_1,q',s)\rho_e(q',t=0)dq'\times\frac{\bar{A}(V_{rg},c_2-q_1,c_2,s)}{\bar{M}(s)}, \tag{15}$$

$$\bar{H}_{rg}(c_2,s)=\bar{H}_{er}(c_1,s)\frac{2\pi V_{er}^2}{\hbar}\frac{\bar{\phi}(c_2-q_1,c_1-q_1,s)}{\bar{A}(V_{rg},c_2-q_1,c_2,s)}=\frac{2\pi V_{er}^2}{\hbar}\frac{\bar{\phi}(c_2-q_1,c_1-q_1,s)}{\bar{M}(s)}\frac{2\pi V_{rg}^2}{\hbar}\times\int_{-\infty}^{\infty}\bar{\phi}(c_1,q',s)\rho_e(q',t=0)dq'. \tag{16}$$

In Eqs. (15) and (16) the following shortened notations are used:

$$\bar{\phi}(x,s)=\bar{\phi}(x,x,s),$$

$$\bar{A}(V,x,y,s)=1+\frac{2\pi V^2}{\hbar}[\bar{\phi}(x,s)+\bar{\phi}(y,s)],$$

$$\bar{B}(V_{er},V_{rg},c_1,c_2,s)=\frac{2\pi V_{er}^2}{\hbar}\frac{2\pi V_{rg}^2}{\hbar}\bar{\phi}(c_1-q_1,c_2-q_1,s)\times\bar{\phi}(c_2-q_1,c_1-q_1,s),$$

$$\bar{M}(s)=\bar{A}(V_{er},c_1,c_1-q_1,s)\bar{A}(V_{rg},c_2-q_1,c_2,s)-\bar{B}(V_{er},V_{rg},c_1,c_2,s).$$

As can be seen from Eqs. (15) and (16) the functions $\bar{H}_{er}(c_1,s)$ and $\bar{H}_{rg}(c_2,s)$ actually depend on the locations of the two crossing points c_1 and c_2. This is due to the term $\bar{B}(V_{er},V_{rg},c_1,c_2,s)$ containing the Laplace transforms of $\phi(c_2-q_1,c_1-q_1,t)$ and $\phi(c_1-q_1,c_2-q_1,t)$. These functions describe the wave packet propagations from c_1 to c_2 and from c_2 to c_1, respectively, on the r potential energy surface. In the following, $\bar{H}_{er}(s)$ and $\bar{H}_{rg}(s)$ will be given by Eqs. (15) and (16), respectively, with the crossing point arguments dropped.

The total populations of each state are given by

$$\rho_x(t)=\int_{-\infty}^{\infty}\rho_x(q,t)dq \tag{17}$$

in the time domain, and

$$\bar{\rho}_x(s)=\int_{-\infty}^{\infty}\bar{\rho}_x(q,s)dq \tag{18}$$

in the Laplace domain. The subscript $x=e$, r or g.

Here we consider the case where the initial distribution of $\rho_s(q,t=0)$ is an equilibrium distribution with respect to the polarization coordinate. Since there is no displacement of the e potential function relative to g potential function, photoexcitation will transfer the equilibrium distribution from the ground state to the excited state. The equilibrium distribution $\rho_e(q,t=0)$ is given by

$$\rho_e(q,t=0)=\exp\left(-\frac{q^2}{2\langle q^2\rangle}\right)\Big/\sqrt{2\pi\langle q^2\rangle}=\phi_{\rm eq}(q). \tag{19}$$

To proceed we use the following identities valid for the Laplace transformed functions:

$$\int_{-\infty}^{\infty} \bar{\phi}(q,q',s)dq = \frac{1}{s}, \tag{20}$$

$$\int_{-\infty}^{\infty} \bar{\phi}(q,q',s)\phi_{eq}(q')dq' = \frac{\phi_{eq}(q)}{s}. \tag{21}$$

Using Eqs. (12), (20). amd (21) we obtain the following solutions in the time domain

$$\rho_e(q,t) = \phi_{eq}(q) - \int_0^t H_{er}(\tau)\phi(q,c_1,t-\tau)d\tau, \tag{22a}$$

$$\rho_r(q,t) = \int_0^t H_{er}(\tau)\phi(q-q_1,c_1-q_1,t-\tau)d\tau, - \int_0^t H_{rg}(\tau)\phi(q-q_1,c_2-q_1,t-\tau)d\tau, \tag{22b}$$

$$\rho_g(q,t) = \int_0^t H_{rg}(\tau)\phi(q,c_2,t-\tau)d\tau, \tag{22c}$$

where $H_{er}(t)$ and $H_{rg}(t)$ are the inverse Laplace transforms of $\bar{H}_{er}(s)$ and $\bar{H}_{rg}(s)$, respectively. These are general solutions of the three-surface problem. The distribution functions, $\rho_x(t,q),(x=s,r,g)$, can be used for the calculation of the time-dependent mean values of the q-dependent observable physical quantities. Below we will be interested in the total population of the initially excited state and the population of the radical–ion pairs.

Using Eqs. (12), (18), and (20)–(22) we obtain the solutions for the total populations in the Laplace domain

$$\bar{\rho}_e(s) = \frac{1}{s} - \frac{\bar{H}_{er}(s)}{s}, \tag{23a}$$

$$\bar{\rho}_r(s) = \frac{\bar{H}_{er}(s)}{s} - \frac{\bar{H}_{rg}(s)}{s}, \tag{23b}$$

$$\bar{\rho}_g(s) = \frac{\bar{H}_{rg}(s)}{s}. \tag{23c}$$

As required, the Laplace transforms of the populations $\rho_x(t)$ satisfies $\bar{\rho}_e(s)+\bar{\rho}_r(s)+\bar{\rho}_g(s) = 1/s$. In the time domain this is equivalent to $\rho_e(t)+\rho_r(t)+\rho_g(t) = 1$. From Eqs. (23a)–(23c) we can write the solution for the total populations of three levels in the time domain:

$$\rho_e(t) = 1 - \int_0^t H_{er}(\tau)d\tau, \tag{24a}$$

$$\rho_r(t) = \int_0^t H_{er}(\tau)d\tau - \int_0^t H_{rg}(\tau)d\tau, \tag{24b}$$

$$\rho_g(t) = \int_0^t H_{rg}(\tau)d\tau. \tag{24c}$$

From Eqs. (15) and (24a) we find that the rate of the recombination of the radical–ion pairs depends on the time evolution of the initial population on e surface. This dependence is contained in the expression for $\bar{H}_{er}(s)$ and it is connected with the fact that each electron transfer is treated as a reversible process.

For the purpose of further discussion it will be instructive to recall the results obtained by Rips and Jortner[49,50] for two-surface systems. For $V_{rg} = 0$ the relaxation of the radical pair to the ground state (recombination) is forbidden. In this case our three-surface kinetic equation reduces to the two-surface equation. From Eq. (15) we find

$$\bar{H}_{er}(s) = \frac{2\pi V_{er}^2}{\hbar}\int_{-\infty}^{\infty} \frac{\bar{\phi}(c_1,q',s)\rho_e(q',t=0)dq'}{\bar{A}(V_{er},c_1,c_1-q_1,s)}. \tag{25}$$

Thus from Eqs. (23a) and (25) the Laplace transform of the population $\rho_e(t)$ is given by

$$\bar{\rho}_e(s) = \frac{1}{s} - \frac{1}{s}\frac{2\pi V_{er}^2}{\hbar}\int_{-\infty}^{\infty} \frac{\bar{\phi}(c_1,q',s)\rho_e(q',t=0)dq'}{\bar{A}(V_{er},c_1,c_1-q_1,s)}. \tag{26}$$

Consider the special case where the initial distribution of the polarization coordinate is $\rho_e(q',t=0) = \delta(q'-q_x)$. From Eq. (26) we obtain

$$\bar{\rho}_e(s) = \frac{1}{s} - \frac{1}{s}\frac{2\pi V_{er}^2}{\hbar}\frac{\bar{\phi}(c_1,q_x,s)}{\bar{A}(V_{er},c_1,c_1-q_1,s)} = \bar{G}_e(s). \tag{27}$$

Equation (27) gives the Laplace transform of the initial state for an initial δ function distribution in q centered at q_x at $t=0$ and reaction occuring at the crossing point c_1. In Eq. (27) these two points appear in the multiplier $\bar{\phi}(c_1,q_x,s)$ in the numerator. The function $\phi(c_1,q_x,t)$ describes the motion of the wave packet from q_x to the crossing point c_1. For a Gaussian equilibrium distribution in q, $\rho_e(q',t=0) = \phi_{eq}(q')$, from Eqs. (21) and (26) we find

$$\bar{\rho}_e(s) = \frac{1}{s} - \frac{1}{s^2}\frac{2\pi V_{er}^2}{\hbar}\frac{\phi_{eq}(c_1)}{\bar{A}(V_{er},c_1,c_1-q_1,s)}. \tag{28}$$

Equations (27) and (28) are identical to those derived by Rips and Jortner for the two-surface system as required.

Returning to the three-level problem, Eq. (24b) can be rewritten in an equivalent form more suitable for physical interpretation. Using Eqs. (16) and (23b) we have

$$\bar{\rho}_r(s) = \bar{H}_{er}(s)\left[\frac{1}{s} - \frac{1}{s}\frac{2\pi V_{rg}^2}{\hbar}\frac{\bar{\phi}(c_2-q_1,c_1-q_1,s)}{\bar{A}(V_{rg},c_2-q_1,c_2,s)}\right], = \bar{H}_{er}(s)\bar{G}_r(s) \tag{29}$$

where

$$\bar{G}_r(s) = \frac{1}{s} - \frac{1}{s}\frac{2\pi V_{rg}^2}{\hbar}\frac{\bar{\phi}(c_2-q_1,c_1-q_1,s)}{\bar{A}(V_{rg},c_2-q_1,c_2,s)}. \tag{30}$$

Comparing Eq. (30) for $\bar{G}_r(s)$ and Eq. (27) for $\bar{G}_e(s)$ we can give an interpretation for $\bar{G}_r(s)$. The function $\bar{G}_r(s)$ represents the Laplace transform of the time-dependent population of the radical pairs for an initial δ-function distribution in q centered at the crossing point c_1 at $t=0$ on the r potential surface and reaction occuring at the crossing point c_2. In Eq. (30) these crossing points appear in the multiplier $\bar{\phi}(c_2-q_1,c_1-q_1,s)$. This factor describes the motion of the wave packet from c_1 to the crossing point c_2. The relaxation function $\bar{G}_r(s)$ is independent of the dynamics occuring on the e potential energy surface. The formation of radical–ion pairs at the point c_1 is described by $H_{er}(t)$.

Equation (29) allows us to write the transient population of the radical pairs in the following form in the time domain

$$\rho_r(t) = \int_0^t H_{er}(\tau) G_r(t-\tau) d\tau. \tag{31}$$

It is the convolution of the source term $H_{er}(t)$ and the population response function for the relaxation of the radical–ion pairs formed at c_1, $G_r(t)$. Below we will show that this form of the expression for the transient population is particularly convenient in the evaluation of the geometrically averaged quantities.

III. NUMERICAL CALCULATIONS

Solvent relaxation influences the kinetics of the radical pairs at long and short times in different ways. At short time, the solvent is still relaxing around the radical–ion pairs. There are two effects here. The first is that ions still near the c_1 crossing point are undergoing significant barrier recrossing. The second is that there is no back transfer until the solvent has relaxed to the c_2 crossing point (see Fig. 1). This gives rise to a fast initial increase in the radical–ion population. At long time, the solvent relaxation is complete and the radical–ion–solvent systems have relaxed to the bottom of the r surface. Thermal fluctuations will be necessary to bring these systems up to the c_2 crossing point so that back transfer can occur (except for the situation of barrierless back transfer). This is a slower process than radical–ion formation and would be responsible for long tails in the radical–ion population.

The solution of the kinetic problem in Sec. II is given in terms of the Laplace transform of the function $\phi(q,q',t)$. This describes the propagation and spreading of the wave packet on three different potential energy surfaces. At very long times ($t \gg \tau_L$), $\phi(q,q',t)$ approaches the equilibrium distribution $\phi_{eq}(q)$. Its Laplace transform was calculated as follows

$$\bar{\phi}(q,q',s) = \frac{\phi_{eq}(q)}{s} + \bar{w}(q,q',s), \tag{32}$$

where

$$\bar{w}(q,q',s) = \int_0^\infty [\phi(q,q',t) - \phi_{eq}(q)] e^{-st} dt. \tag{33}$$

For $q = q'$ we use the shortened notation $\bar{w}(q,q,s) = \bar{w}(q,s)$. The Laplace transform $\bar{w}(q,q',s)$ was evaluated by numerical integration using Gaussian quadrature.

Using Eqs. (22), (32), and (33) the Laplace transforms of the relaxation functions, $\bar{G}_e(s)$ and $\bar{G}_r(s)$, can be written in the following form:

$$G_e(s) = \frac{1}{s} - \left[\frac{\bar{k}_{1f}(s)}{s + k_1(s)}\right]\left[\frac{\bar{\phi}(c_1,q_x,s)}{\phi_{eq}(c_1)}\right], \tag{34}$$

$$G_r(s) = \frac{1}{s} - \left[\frac{\bar{k}_{2f}(s)}{s + k_2(s)}\right]\left[\frac{\bar{\phi}(c_2 - q_1, c_1 - q_1, s)}{\phi_{eq}(c_2 - q_1)}\right], \tag{35}$$

where the Laplace transforms of the time dependent rate coefficients[36,39] for forward (f) and back (b) electron transfer processes at the crossing points c_1 and c_2, respectively, are given by

$$\bar{k}_{1f}(s) = \left[\frac{2\pi V_{er}^2}{\hbar}\right]\frac{\phi_{eq}(c_1)}{1 + \bar{\kappa}_A(V_{er},s)}, \tag{36a}$$

$$\bar{k}_{1b}(s) = \left[\frac{2\pi V_{er}^2}{\hbar}\right]\frac{\phi_{eq}(c_1 - q_1)}{1 + \bar{\kappa}_A(V_{er},s)}, \tag{36b}$$

$$\bar{k}_{2f}(s) = \left[\frac{2\pi V_{rg}^2}{\hbar}\right]\frac{\phi_{eq}(c_2 - q_1)}{1 + \bar{\kappa}_A(V_{rg},s)}, \tag{36c}$$

$$\bar{k}_{2b}(s) = \left[\frac{2\pi V_{rg}^2}{\hbar}\right]\frac{\phi_{eq}(c_2)}{1 + \bar{\kappa}_A(V_{rg},s)}, \tag{36d}$$

where

$$\bar{\kappa}_A(V_{er},s) = \frac{2\pi V_{er}^2}{\hbar}[\bar{w}(c_1,s) + \bar{w}(c_1 - q_1,s)], \tag{37a}$$

$$\bar{\kappa}_A(V_{rg},s) = \frac{2\pi V_{rg}^2}{\hbar}[\bar{w}(c_2 - q_1,s) + \bar{w}(c_2,s)], \tag{37b}$$

and

$$\bar{k}_1(s) = \bar{k}_{1f}(s) + \bar{k}_{1b}(s), \tag{38a}$$

$$\bar{k}_2(s) = \bar{k}_{2f}(s) + \bar{k}_{2b}(s). \tag{38b}$$

The values of the intermediate functions $\bar{\kappa}_A(V_{er},s)$ and $\bar{\kappa}_A(V_{rg},s)$ given by Eqs. (37a) and (37b) for the Laplace transform parameter $s = 0$ represent the adiabaticity parameters for the forward and reverse electron transfer processes,[38,39] respectively.

The source function $\bar{H}_{er}(c_1,s)$ has the following form:

$$\bar{H}_{er}(c_1,s) = \left[\frac{\bar{k}_{1f}(s)}{s + \bar{k}_1(s)}\right]\left[\frac{1}{1 - \bar{D}(s)}\right], \tag{39}$$

where

$$\bar{D}(s) = \left[\frac{\bar{k}_{1b}(s)}{s + \bar{k}_1(s)}\frac{\bar{k}_{2f}(s)}{s + \bar{k}_2(s)}\right] \times \left[1 + s\frac{\bar{w}(c_1 - q_1, c_2 - q_1, s)}{\phi_{eq}(c_1 - q_1)}\right] \times \left[1 + s\frac{\bar{w}(c_2 - q_1, c_1 - q_1, s)}{\phi_{eq}(c_2 - q_1)}\right]. \tag{40}$$

$\bar{D}(s)$ gives significant contributions where ΔG_r is close to zero and the rate of radical–ion formation is small. If we are interested in ultrafast kinetics with fast forward electron transfer then $\bar{k}_{1b}(s) \ll \bar{k}_1(s)$ and we can neglect this term and the following formula gives a reasonable approximation for the source function

$$\bar{H}_{er}(s) = \frac{\bar{k}_{1f}(s)}{s + \bar{k}_1(s)}. \tag{41}$$

Applying the inverse Laplace transformation on Eqs. (35) and (31) we obtain, respectively,

$$G_r(t) = 1 - \int_0^t L_1(t')\left[\frac{\phi(c_2 - q_1, c_1 - q_1, t - t')}{\phi_{eq}(c_2 - q_1)}\right] dt', \tag{42}$$

$$\rho_r(t) = \int_0^t H_{er}(\tau) G_r(t-\tau) d\tau, \tag{43}$$

where

$$L_1(t') = L^{-1}\left[\frac{\bar{k}_{2f}(s)}{s + \bar{k}_2(s)}\right].$$

The relaxation functions $G_e(t)$, $G_r(t)$ and the source function $H_{er}(t)$, are given in terms of inverse Laplace transforms of the functions of the Laplace transforms of time dependent rate coefficients. The nature of the processes occuring at the crossing points c_1 and c_2 is determined at long times by the adiabaticity parameters $\bar{\kappa}_A(V_{er},0)$ and $\bar{\kappa}_A(V_{rg},0)$, respectively. As can be seen from Eq. (33), the functions $\bar{w}(c_1,0)$ and $\bar{w}(c_1-q_1,0)$, entering the definition of the adiabaticity parameter $\bar{\kappa}_A(V_{er},0)$, are proportional to the average times (defined as zero-order moments) it takes for a solvent fluctuation at the crossing point c_1 to relax to thermal equilibrium in the s state and the r state, respectively. Similarly, $\bar{w}(c_2-q_1,0)$ and $\bar{w}(c_2,0)$ are proportional to the average escape times for the δ-function-like wave packet at c_2 to relax to thermal equilibrium in the r and g wells, respectively. When $\bar{\kappa}_A(V,0) \ll 1$ the reaction is nonadiabatic and the rates are given by $\bar{k}_{1f}(0) = (2\pi V_{er}^2/\hbar)\phi_{eq}(c_1)$ and $\bar{k}_{2f}(0) = (2\pi V_{rg}^2/\hbar)\phi_{eq}(c_2-q_1)$, they are independent of the dielectric relaxation properties of the solvent (long time limit). In the opposite limit, $\bar{\kappa}_A(V,0) \gg 1$, the reaction is adiabatic and the rates are determined by the inverse of the sum of the average time it takes to escape from the crossing point of two adjacent potential wells.

In the calculation of the inverse Laplace transforms of $\bar{k}_{2f}(s)/[s+\bar{k}_2(s)]$ and $\bar{H}_{er}(s)$ the Stehfest algorithm was used.[62] The arguments of the function $\phi(q,q',t)$ are defined as follows: c_1 is the first crossing point measured relative to minimum of the e surface; c_1-q_1 and c_2-q_1 are the coordinates of the first crossing point relative to the miminum of the r surface and the coordinate of the second crossing point relative to the minimum of g surface, respectively (see Fig. 1); and t is the time. Since $q_1 = 2\lambda$, from Eqs. (2) and (3) we obtain

$$c_1 = +\lambda + \Delta G_r, \tag{44}$$

$$c_1 - q_1 = -\lambda + \Delta G_r, \tag{45}$$

$$c_2 - q_1 = -\lambda + \Delta G_r - \Delta G_g, \tag{46}$$

$$c_2 = +\lambda + \Delta G_r - \Delta G_g. \tag{47}$$

The calculations were performed on a DEC station 3100 computer and the programs were written in C.[63] To calculate the inverse Laplace transform at time t the Laplace transformed function was evaluated at 18 points (as required by the Stehfest algorithm for double precision floating point numbers). However, for each calculation care must be taken to make sure all points are accurate and do not suffer from round-off error. Round-off error is demonstrated by rapid, almost oscillatory appearing fluctuations in the results. If an inverse transform had fluctuations we recalculated the integrals at a higher accuracy until the inverse transforms were smooth. While any form of the solvent relaxation can be used, the calculations presented here were performed for a Debye solvent with a single relaxation time. The solvent correlation function was a single exponential

$$\Delta(t) = \exp(-t/\tau_L), \tag{48}$$

where τ_L is the longitudinal relaxation time.

The natural log of the source function $H_{er}(t)$ is shown for a variety of parameters in Fig. 2. The parameters are given in the figure caption. The magnitude of the source function $H_{er}(t)$ is determined by the net transfer of probability from the e surface to the r surface at the crossing point c_1. It is dominated by the time-dependent probability of moving to point c_1. At $t=0$ there is some probability of being at c_1, so there is initially very fast transfer from e to r. Later on, the rate of probability transfer decreases because of the need to reach c_1 on the e surface and recrossing from the r surface. This can be seen in the steep slopes at short times, and the smaller slopes at long times, for each curve in Fig. 2. All curves at long time are straight lines which means that the source function in the long time limit is exponential. This can be seen by looking at Eq. (A1) in Appendix A, which is the source function in the long time limit. It should be noted that the curves A, B, and C are in the normal region, curve D is barrierless and curve E is in the inverted region (see Fig. 1). Curves C and E are similar because they are equidistant yet are on opposite sides of the normal-inverted region border. This means they should have similar electron transfer rates. They are slightly different because curves C and E have different crossing points between the r and g surfaces.

In Fig. 3 the natural logs of the relaxation function $G_r(t)$ are shown for different parameters. They are strongly dependent on the free energy differences between the r and g states, and the exact location of the crossing points on the r potential function. The relaxation function determines the dynamics of solvation and the recombination reaction (at point c_2, see Fig. 1) to the ground state. In each curve there is an "induction" time before the solvent dynamics carries the ion–solvent system to the next crossing point., The wave packet starts on r at c_1. As the wave packet moves down the potential surface it also spreads. Until the leading edge of the packet reaches c_2, no relaxation from r to g occurs, and $G_r(t)$ does not decay. Once the leading edge of the packet reaches c_2, crossing can occur onto the g surface. Back crossing from g to r can also take place as the packet now on g travels down the g surface away from c_2. Curves A, B, and C are in the inverted region for crossing from r to g (at c_2). As ΔG_r decreases going from A to D, the rate of decay of $G_r(t)$ increases. Solvent relaxation brings the packet to the botom of

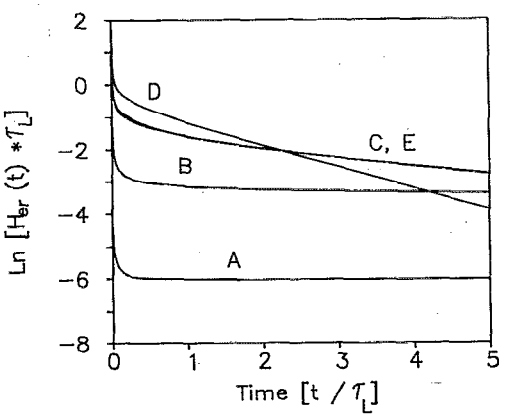

FIG. 2. The time dependence of the source function $H_{er}(t)$ for different exothermicities of the forward electron transfer reaction. The curves A–E have the following values for ΔG_r: A = −0.25, B = −0.50, C = −0.75, D = −1.00, E = −1.25 eV. The other parameters are $\Delta G_g = -2.0$ eV, $\tau_L = 10$ ps, $\lambda = 1.0$ eV, $T = 300$ K, $V_{er} = 0.01$ eV, $V_{rg} = 0.001$ eV.

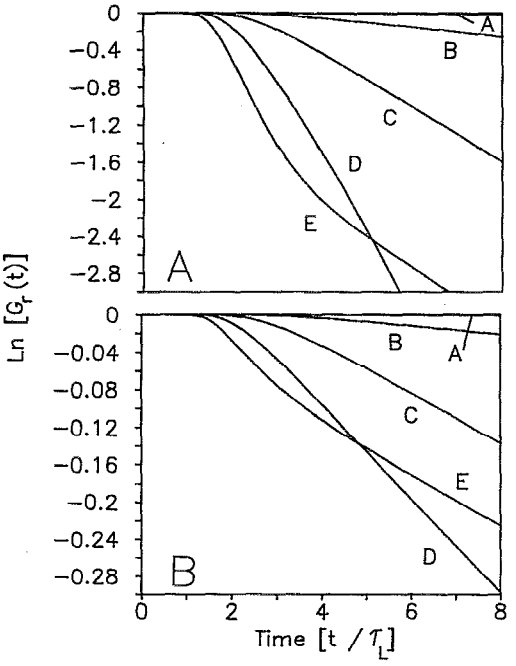

FIG. 3. The time dependence of the relaxation function $G_r(t)$ for different exothermicities of the forward electron transfer reaction. (A) $V_{er} = V_{rg} = 0.01$ eV, (B) $V_{er} = 0.01$ eV, $V_{rg} = 0.001$ eV. The other parameters are the same as in Fig. 2.

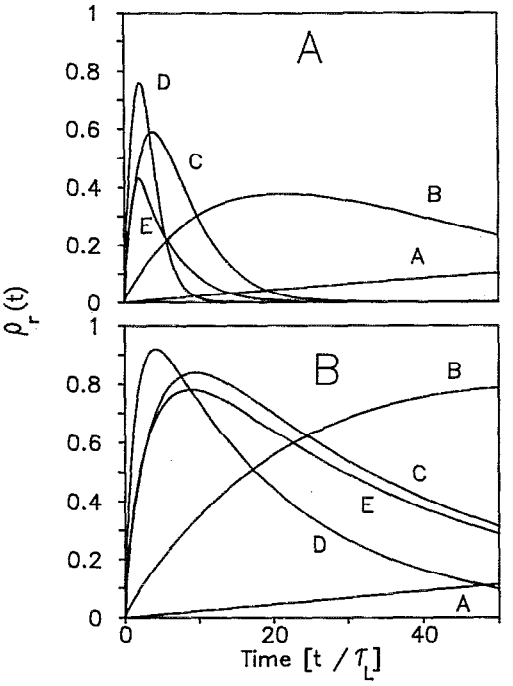

FIG. 4. (A) the transient population of the radical pairs when forward and back electron transfer processes are in the adiabatic limit. (B) The transient population of the radical pairs when forward electron transfer is in the adiabatic limit and the back electron transfer process is nonadiabatic. The parameters are the same as in Fig. 3.

the well. A is a case where c_2 is so far up the well in the inverted region that only the very low amplitude tail of the equilibrated packet reaches c_2. Therefore, the decay is very slow. The packet overlaps c_2 for B and C with increasing amplitude, and the decays are faster. D is the barrierless case, with c_2 at the bottom of the well, so it has the greatest overlap with the equilibrated packet. Curve E has the $r-g$ crossing point in the normal region. The packet reaches c_2 the fastest, so E has the shortest induction time and the steepest early time slope. However, the packet passes by c_2 in going to the bottom of the well, so at long time the r to g relaxation slows. In Fig. 3(A) there are greater rates of decrease in the relaxation function than in Fig. 3(B). In Fig. 3(A) both the forward and back electron transfers were in the adiabatic limit. In Fig. 3(B), the back reaction is nonadiabatic. This is determined by the choice of electronic coupling matrix elements (V_{er} and V_{rg}) between the donor and acceptor electronic states.

The parameters used in Figs. 3–5 are the electronic coupling matrix elements $V_{er} = 0.01$ eV and $V_{rg} = 0.01$ eV for Figs. 3(A) and 4(A), and $V_{rg} = 0.001$ eV for Figs. 3(B) and 4(B). The solvent relaxation time, $\tau_L = 10$ ps, the temperature, $T = 300$ K, the outer sphere reorganization energy, $\lambda = 1.0$ eV, and the curves labeled A–E have the following values for ΔG_r: -0.25, -0.50, -0.75, -1.00, and -1.25 eV.

Figures (4A) and (4B) show the radical–ion populations. The radical–ion populations are obtained from the convolution of the source function $H_{er}(t)$ and the relaxation function $G_r(t)$ [see Eq. (43)]. These curves were calculated with the same parameters as used in Figs. 3(A) and 3(B). In

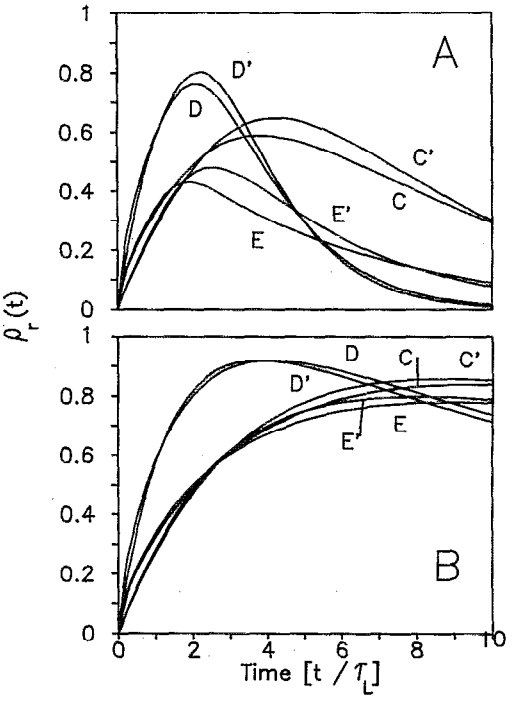

FIG. 5. The transient population of the radical pairs calculated using the exact formula and the approximate formula given by Eq. (A3). (A) Forward and back electron transfer steps are adiabatic. (B) Forward electron transfer is adiabatic the back electron transfer is nonadiabatic. Curves C, D, and E are exact while curves C', D', and E' were calculated using Eq. (A3). The parameters are the same used in Fig. 3.

Fig. 4(A) the results are shown when both the forward and the recombination process are in the adiabatic limit [$V_{rg} = 0.01$ eV (80 cm^{-1})] whereas those in Fig. 4(B) correspond to the case when the forward electron transfer process is adiabatic and recombination is nonadiabatic, $V_{rg} = 0.001$ eV (8 cm^{-1}). In each case the wave packet on the r surface moves from c_1 to c_2 and this distance is equal to ΔG_g. The curve (D) in Figs. 4(A) and 4(B) correspond to the case where both forward and reverse electron transfer steps are barrierless. The crossing points are at the minima of the e and r potential wells. The control of the growth and the decay of the population of the radical–ion pairs by solvent relaxation is the strongest when there are low barriers to electron transfer. Specific transient effects for the radical–ion population can be seen on the time scale of a few τ_L. For larger barriers the long time approximation for the rate coefficient can give a satisfactory description of the time dependence of the radical–ion population.

The model presented above shows that the initial conditions and the wave packet propagation are important for the time dependence of the transient populations at very short times (comparable to a few τ_L). For the equilibrium initial distribution in the polarization coordinate these transient effects are relatively small. For the radical pairs the transient effects are particularly important because the radicals formed at the c_1 crossing point have a δ-function-like distribution in the reaction coordinate. The wave packet spreads and moves from c_1 to the bottom of the potential well. The decay of the radical pairs depend on the exact location of the second crossing point c_2. If c_1 and c_2 are located on the same side of the potential function r then the relaxation is more efficient at short times as the wave packet passes over the crossing point. If c_1 and c_2 are located on opposite sides of the potential well, the time of the transition between these two points is longer. Back electron transfer is less efficient although, in this case, at long time, the rate constants are the same for the crossing points c_1 and c_2.

The model considered here neglects the effects connected with the intramolecular degrees of freedom. The electron transfer event is accompanied by displacement in the equilibrium nuclear coordinates of the products relative to those of reactants. A simple model describing the effect of the intramolecular degrees of freedom was given by Sumi and Marcus.[55] They used harmonic potential energy surfaces in two dimensions, one for the intramolecular coordinate, the other for the solvent polarization coordinate. The product potential energy surface is displaced both in the nuclear coordinate Q and polarization coordinate q relative to the potential energy surface of the reactants. Our case corresponds to zero displacement in the nuclear coordinate ("narrow reaction window"). The crossing of the saddle point on the q axis gives a very narrow initial distribution in the q coordinate on the product potential energy surface. In the case of finite displacement in Q the crossing of the barrier can occur over a broader range in the q coordinate. This gives a broader initial wave packet on the product potential surface. These considerations suggest that the width of the initial distribution on the r potential energy surface is always narrower than the initial equilibrium distribution on the reactant potential energy surface. This situation would be expected for electron transfer reactions in polar solvents. Although the above arguments should be valid for reactions at fixed distance, additional effects should be taken into account in the analysis of situations in which there is a spread of distances or orientations. The electron transfer probabilities are distance dependent (and orientation dependent) due to the distance dependence of the electronic coupling matrix element $V(\mathbf{R})$ and the solvent reorganization energy $\lambda(\mathbf{R})$. The latter factor determines the displacement of the potential energy surfaces of the products and reactants.

Recently, Lin *et al.*[56,58] have modeled the transient population of radical–ion pairs for the three-surface system for a system of a donor and many acceptors. They included the influence of the random spatial distribution of acceptors. They assumed nonadiabatic electron transfer processes occuring between the $s - r$ and $r - g$ surfaces and solvation dynamics on the r surface. Back electron transfer can occur at any state of solvent relaxation with the rate constant dependent on the vertical energy difference. They pointed out that the method used for spatial averaging could be extended to other models of solvent relaxation. The model presented here takes into account the solvent dynamics on all three surfaces allowing us to include, in a simple way, the adiabaticity effects for forward and back electron transfer processes. However, the calculations are for a single molecular pair at a single spearation (see Appendix B for formal considerations for spatial averaging). The results of this paper confirm the importance of the ion solvation dynamics on the r surface for the time dependence of the radical–ion population. These dynamics determine the time dependence of the relaxation function $G_r(t)$. The inclusion of solvation effects on the e surface has given rise to an additional effect. Solvation dynamics on the initial e surface and at the first crossing point c_1 determine the short time dependence of the source function $H_{er}(t)$. The growth of the population is amplified by the delay in back electron transfer to the ground state at short times. This is due to the finite rate of the wave packet motion away from the c_1 crossing point. The combined effect gives a fast initial increase in the radical–ion pair population which may be followed by slower growth of the population if the back transfer is slow. These features were observed in recent femtosecond–picosecond laser photolysis studies on the dynamics of ion-pair formation in the excited state of tetracyanobenzene–aromatic hydrocarbon complexes in polar solvents.[59]

One would expect that the initial distribution of the reaction coordinate on the initial e surface, other than the equilibrium distribution, should have a strong influence on this short time behavior of the source function. Such a situation occurs when there is substantial displacement of the e potential surface relative to the ground state surface g, e.g., systems where large Stokes shifts of the absorption and fluorescence transitions from the e state to the g state are present.

IV. CONCLUDING REMARKS

The solution of the Zusman-type equations for the three-surface system has been presented. The model de-

scribes ultrafast formation and recombination of radical–ion pairs limited by solvent dielectric relaxation. The solvent relaxation properties can be taken into account using the polarization coordinate autocorrelation function $\Delta(t)$. The theory applies to the electron transfer processes between excited electron donor/acceptor and electron acceptor/donor separated by constant distance. The theory can also be applied to intermolecular reactions in systems of any geometry in the absence of translational motion of the reactants and products. Because solvent relaxation occurs very rapidly, the neglect of diffusion may not significantly effect the results on relevant time scales. On longer time scales, where solvent relaxation has occurred, electron transfer and back transfer with diffusion has been treated.[61,64] Using procedures based on the numerical inverse Laplace transformation we analyzed time dependences of the rate of radical–ion pair formation $H_{er}(t)$, the relaxation function $G_r(t)$ describing the time evolution of the radical recombination, and finally, the transient populations of the radical–ion pairs. We demonstrated the importance of the initial conditions and the sensitivity to the crossing points on the potential sufaces on the time evolution of the transient population of the radical–ion pairs.

ACKNOWLEDGMENTS

This work was supported by the Department of Energy, Office of Basic Energy Sciences (DE-FG03-84ER13251). J.N. thanks the Polish Academy of Sciences (CPBP 01.19) for partial support. Computing equipment was provided by the National Sciences Foundation computing grant (CHE88-21737).

APPENDIX A

For solvent controlled electron transfer, the dominant factor is the propagation of the wave packet, $\phi(c_2-q_1, c_1-q_1,t)$, on the r potential surface between the crossing points c_1 and c_2. In Sec. III, it was shown that the contribution of the term $\bar{D}(s)$ to the source function $\bar{H}_{er}(s)$ is of secondary importance, and in many cases can be neglected. A useful and simple formula for the transient radical–ion population can be derived using the long time approximation for the rate coefficients [Eqs. (36)–(38)] and using Eq. (41) for the source function $\bar{H}_{er}(s)$. The long time approximation corresponds to setting $s=0$ in the expressions for the rate coefficients [Eqs. (36)–(38)]. Performing the inverse Laplace transform on Eq. (41) we obtain

$$\bar{H}_{er}(t) = k_{1f}^{\infty} \exp(-k_1^{\infty} t). \tag{A1}$$

Equation (42) can be written in the following form:

$$G_r(t) = 1 - \int_0^t k_{2f}^{\infty} \exp(-k_2^{\infty} t') \times \frac{\phi(c_2-q_1, c_1-q_1, t-t')}{\phi_{eq}(c_2-q_1)}\, dt'. \tag{A2}$$

From Eqs. (43), (A1), and (A2) we obtain

$$\rho_r(t) = \frac{k_{1f}^{\infty}}{k_1^{\infty}}[1-\exp(-k_1^{\infty} t)] - k_{1f}^{\infty} k_{2f}^{\infty} \times \int_0^t \int_0^{\tau} \exp[-k_1^{\infty}(t-\tau)] \times \left[\frac{\phi(c_2-q_1, c_1-q_1, \tau-t')}{\phi_{eq}(c_2-q_1)}\right] \times \exp(-k_2^{\infty} t')\, dt'\, d\tau, \tag{A3}$$

where $k_t^{\infty} = \bar{k}_1(0)$, $k_2^{\infty} = \bar{k}_2(0)$, $k_{1f}^{\infty} = \bar{k}_{1f}(0)$ and $k_{2f}^{\infty} = \bar{k}_{2f}(0)$.

Equation (A3) can be evaluated more easily by numerical methods than Eq. (43) because only the long time values of the rate coefficients k_1^{∞}, k_2^{∞}, k_{1f}^{∞}, and k_{2f}^{∞} need to be evaluated when Eq. (A3) is used.

Finally applying the long time approximation to $\phi(c_2, -q_1, c_1-q_1, \tau-t')$, which for $t \gg \tau_L$ is equal to $\phi_{eq}(c_2, -q_1)$, from Eq. (A2); we obtain

$$G_r(t) = 1 - \int_0^t k_{2f}^{\infty} \exp(-k_2^{\infty} t')\, dt' = 1 - \frac{k_{2f}^{\infty}}{k_2^{\infty}}[1-\exp(-k_2^{\infty} t)] \tag{A4}$$

and from Eq. (A3) we get

$$\rho_r(t) = \left[\frac{(k_2^{\infty} - k_{2f}^{\infty}) k_{1f}^{\infty}}{k_1^{\infty} k_2^{\infty}}\right][1-\exp(-k_1^{\infty} t)] + \left[\frac{k_{1f}^{\infty} k_{2f}^{\infty}}{k_2^{\infty}(k_1^{\infty} - k_2^{\infty})}\right] \times [\exp(-k_2^{\infty} t) - \exp(-k_1^{\infty} t)] \tag{A5}$$

when k_1^{∞} is not equal to k_2^{∞}.

$$\rho_r(t) = \left[\frac{(k_1^{\infty} - k_{1f}^{\infty}) k_{1f}^{\infty}}{(k_1^{\infty})^2}\right][1-\exp(-k_1^{\infty} t)] + \left[\frac{(k_{1f}^{\infty})^2}{k_1^{\infty}} t\right]\exp(-k_1^{\infty} t) \tag{A6}$$

for the case when $k_1^{\infty} = K_2^{\infty}$. When the rate coefficients for reverse reaction occuring at the crossing points c_1 and c_2 are neglected [$\bar{k}_{1r}(0) = \bar{k}_{2r}(0) = 0$] then from Eq. (A5) we obtain the well-known result for the transient kinetics.

$$\rho_r(t) = \left[\frac{k_{1f}^{\infty}}{k_1^{\infty} - k_2^{\infty}}\right][\exp(-k_2^{\infty} t) - \exp(-k_1^{\infty} t)] \tag{A7}$$

whereas from Eq. (A6) we get

$$\rho_r(t) = k_1^{\infty} t \exp(-k_1^{\infty} t). \tag{A8}$$

Equations (A5) and (A6) describe the transient kinetics using rate constants for the case when the forward and recombination processes are reversible.

In Figs. 5 and 6 the results of the calculations for the radical–ion population at short times ($< 10\tau_L$) are given. The exact formula, Eq. (43) is used as well as two levels of approximation given by Eqs. (A3) (in Fig. 5), and (A5) or (A6) (in Fig. 6). The approximate formula Eq. (A3) takes into account solvation dynamics on the r surface but uses the

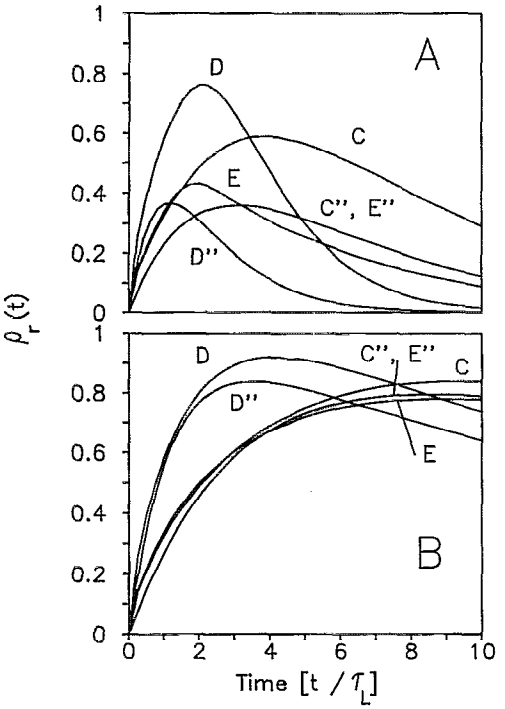

FIG. 6. The transient population of the radical pairs calculated using the exact formula and the most approximate formulae given by Eqs. (A5) and (A6). (A) Forward and back electron transfer steps are adiabatic. (B) Forward electron transfer is adiabatic limit the back electron transfer is nonadiabatic. Curves C, D, and E are exact while curves C", D", and E" were calculated using Eqs. (A5) and (A6). The parameters are the same used in Fig. 3.

long time approximation for the rates of the forward and back electron transfer steps occuring at the c_1 and c_2 crossing points. The comparison is shown for ΔG_{er} equal to C) -0.75, D) -1.00, and E) -1.25 eV where the influence of the solvent relaxation properties on the kinetics is the strongest. When Eq. (A3) is used some features of the population growth connected with the fast nonstationary portion of the source function are lost. The differences between the transient populations calculated from Eqs. (43) and (A3) are larger for the case when the back electron transfer is fast (Fig. 5A) than when the back electron transfer is slow (Fig. 5B). The predictions based on Eq. (A3) overestimate the maximum population of the radical–ion pairs for the case shown in Fig. 5(A). However, if we apply the approximation leading to Eqs. (A5) and (A6) the predictions plotted in Fig. 6(A) show that this approximation is very bad. When the solvation dynamics on the r surface are neglected even the difference between cases C and E is lost, the curves C" and E" are identical in Fig. 6.

APPENDIX B

In Sec. II the formulae for the transient populations of the initial state and the radical–ion state assuming constant separation of the reacting species were derived. Constant separation of donors and acceptors is the case for intramolecular electron transfer reactions when the subunits are separated by rigid spacers. For flexible spacers or in a solution of randomly distributed donors and acceptors our results have to be averaged over the distance distribution. For donor/acceptor random solutions, interactions of many quencher molecules with the excited molecule have to be taken into account.[53–62] The distance dependence of the transients is connected with the distance dependence of the electronic coupling matrix elements $V_{er}(\mathbf{R})$, $V_{rg}(\mathbf{R})$ and the reorganization energy $\lambda(\mathbf{R})$.

Here we present some formal considerations pertaining to this problem. Let the excited molecule be located at the coordinate origin and the quencher molecules occupy the lattice sites characterized by the position vectors $\mathbf{R}_i$.[52–54] There are N sites accessible for the quencher molecules. These sites can be occupied by the quencher molecule with some probability p_i depending on the quencher concentration and the position of site i. These sites can be on a lattice of any form and geometry. The lattice can be finite or infinite in size and can have any dimensionality. Lattice models can be applied to small systems, micelles, polymer coils, interfaces, crystals, or bulk solutions. The geometry of the system can be specified to any degree of accuracy. Finite size of the molecules can be taken into account properly in a simple fashion.[56,60] Assuming that the electron transfer processes between the excited molecule and n different quencher molecules, having configuration $\{\mathbf{R}\}$, are mutually independent we can write for the probability that the molecule excited at $t=0$ is in the excited state at time t as

$$\rho_e(\{\mathbf{R}_i\},t) = \exp(-t/\tau) \prod_{i=1}^{n} \rho_e(\mathbf{R}_i,t), \tag{B1}$$

where τ is the relaxation time of the excited molecule in the absence of the quencher molecules. Here we apply the generalized binomial distribution for the calculation of the ensemble averages.[60] The probability $P_{n,m}$ of a configuration with n quencher molecules occupying N sites is given by

$$p_{n,m} = \prod_{i\in n,m}^{n} p_i \prod_{i\notin n,m}^{N-m} [1-p_i], \quad m = 1,\ldots,\binom{N}{n}. \tag{B2}$$

The multiplier $1-p_i$ giveds the probability that site i is not occupied by the quencher. The subscript m distinguishes between different distributions of n quenchers over N sites. The mean value of a function $K_{n,m}$ that depends on the configuration of quencher molecules $\{\mathbf{R}_i\}$ is given by the following expression:[52,60]

$$\langle K \rangle = \sum_{n=0}^{N} \sum_{m=1}^{\binom{N}{n}} K_{n,m} P_{n,m}. \tag{B3}$$

It can be shown[52,60] using Eqs. (B1)–(B3) that the mean value of the initial state population is given by

$$\langle \rho_e(t) \rangle = \exp(-t/\tau) \prod_{i=1}^{N} [1-p_i+\rho_e(\mathbf{R}_i,t)], \tag{B4}$$

where the product runs over all sites and each site is counted only once. Equation (B4) is formally valid for all concentrations of the quencher molecules including the case $p=1$ (this is where all sites are filled with quenchers). Using Eq. (B4) for the relaxation rate of the mean population of the initial state we obtain

$$-\frac{d\langle\rho_e(t)\rangle}{dt}=\frac{1}{\tau}\langle\rho_e(t)\rangle-\sum_{i=1}^{N}p_i\left[\frac{\partial\rho_e(\mathbf{R}_i,t)}{\partial t}\right]\times\left[\frac{\langle\rho_e(t)\rangle}{1-p_i+p_i\rho_e(\mathbf{R}_i,t)}\right]. \quad \text{(B5)}$$

The first term $(1/\tau)\langle\rho_e(t)\rangle$ gives the probability of direct relaxation of the initial state to the ground state. The second term gives the rate of the radical pair formation $P_e(t)$. Using Eq. (24a), this term can be written in the following form:

$$P_e(t)=\sum_{i=1}^{N}P_e(\mathbf{R}_i,t), \quad \text{(B6)}$$

where

$$P_e(\mathbf{R}_i,t)=p_iH_{er}(t)\left[\frac{\langle\rho_e(t)\rangle}{1-p_i+p_i\rho_e(\mathbf{R}_i,t)}\right] \quad \text{(B7)}$$

represents the probability of radical formation on the site i at position $\mathbf{R}_i$ at time t. As a result of forward electron transfer only one radical pair is created which subsequently recombines to form the ground state product.[56] The probability of finding the radical pair separated by the distance $\mathbf{R}_i$ at time t, $\langle\rho_r(\mathbf{R}_i,t)\rangle$, can be given as convolution of the radical formation rate, $P_e(\mathbf{R}_i,t)$, and the population response function, $G_r(\mathbf{R}_i,t)$, [see Eq. (32) for the single pair case]. We obtain

$$\langle\rho_r(\mathbf{R}_i,t)\rangle=\int_0^t P_e(\mathbf{R}_i,\tau)G_r(\mathbf{R}_i,t-\tau)d\tau. \quad \text{(B8)}$$

Equation (B8) permits for analysis of the time evolution of the distance distributions of germinate radical pairs.

The total mean population of the radical pairs is

$$\langle\rho_r(t)\rangle=\sum_{i=1}^{N}\langle\rho_r(\mathbf{R}_i,\tau)\rangle=\sum_{i=1}^{N}\int_0^t P_e(\mathbf{R}_i,\tau)G_r(\mathbf{R}_i,t-\tau)d\tau. \quad \text{(B9)}$$

In the three-dimensional case with spherical symmetry, a continuous distribution of sites characterized by the distribution function $g(R)$, and the distance dependent occupancies $p(R)$, Eqs. (B4) and (B9) can be given in more explicit forms. Taking the thermodynamic limit, $N,V\to\infty$, $N/V\to\rho$, where ρ is the mean density of sites we obtain

$$\langle\rho_e(t)\rangle=\exp(-t/\tau)\exp\{4\pi\rho\int_a^\infty \ln[1-p(R)+p(R)\rho_e(R,t)]g(R)R^2dR\} \quad \text{(B10)}$$

$$\langle\rho_r(R,t)\rangle=\int_0^t\frac{p(R)H_{er}(R,\tau)\langle\rho_e(\tau)\rangle}{1-p(R)+p(R)\rho_e(R,t)}G_r(R,t-\tau)dr \quad \text{(B11)}$$

and

$$\langle\rho_r(t)\rangle=4\pi\rho\int_a^\infty\langle\rho_r(R,t)\rangle g(R)R^2dR. \quad \text{(B12)}$$

These two formulas generalize the results obtained in previous theoretical considerations on nonadiabatic electron transfer reactions.[56–62] The generalized binomial distribution used above can be applied to systems other than those with random distributions with the geometrical structure characterized by the radial distribution of sites, $g(R)$ and the occupancies described by the function $p(R)$.

[1] M. D. Newton and N. Sutin, Annu. Rev. Phys. Chem. **35**, 437 (1984).
[2] R. A. Marcus Commemorative Issue, J. Phys. Chem. **90**, 3657–3862 (1986).
[3] K. V. Mikkelsen and M. A. Ratner, Chem. Phys. **87**, 113 (1987).
[4] U. S. Steiner, and T. Ulrich, Chem. Rev. **89**, 51 (1989).
[5] G. Fleming, Annu. Rev. Phys. Chem. **37**, 105 (1986).
[6] Y. R. Shen, *The Principles of Nonlinear Optics* (Wiley, New York, 1984).
[7] A. Laubereau and W. Kaiser, Rev. Mod. Phys. **50**, 607 (1978).
[8] M. D. Fayer, Annu. Rev. Phys. Chem. **33**, 63 (1982).
[9] G. R. Fleming, *Chemical Applications of Ultrafast Spectroscopy* (Oxford, University, New York, 1986).
[10] B. Bagchi, Annu. Rev. Phys. Chem. **40**, 115 (1989).
[11] W. Coffey, Adv. Chem. Phys. **63**, 69 (1985).
[12] S. Mukamel, Adv. Chem. Phys. **70**, 165 (1988).
[13] R. A. Marcus, J. Chem. Phys. **24**, 966 (1956).
[14] R. A. Marcus, Annu. Rev. Phys. Chem. **15**, 155 (1964).
[15] N. R. Kastner, J. Logan, and J. Jortner, J. Phys. Chem. **78**, 2148 (1974).
[16] J. Jortner, J. Chem. Phys. **64**, 4860 (1976).
[17] S. H. Northrup and J. T. Hynes, J. Chem. Phys. **73**, 2700 (1980).
[18] R. Grote and J. T. Hynes, J. Chem. Phys. **73**, 2715 (1980).
[19] G. van der Zwan and J. T. Hynes, J. Chem. Phys. **76**, 2993 (1982); **78**, 4174 (1983).
[20] G. van der Zwan and J. T. Hynes, J. Phys. Chem. **89**, 4181 (1985).
[21] J. T. Hynes, Annu. Rev. Phys. Chem. **36**, 573 (1985).
[22] J. T. Hynes, J. Phys. Chem. **90**, 3701 (1986).
[23] M. Maroncelli and G. R. Fleming, J. Chem. Phys. **89**, 875 (1988).
[24] J. Straub and B. Berne, J. Chem. Phys. **85**, 2999 (1986).
[25] G. L. Closs, L. T. Calcaterra, N. J. Green, K. W. Penfield, and J. R. Miller, J. Phys. Chem. **90**, 3673 (1986).
[26] E. M. Kosower and D. Huppert, Annu. Rev. Phys. Chem. **37**, 127 (1986).
[27] P. F. Barbara and W. Jarzeba, Adv. Photochem. **15**, 1 (1900).
[28] D. Calef and P. G. Wolynes, J. Chem. Phys. **78**, 4145 (1983).
[29] P. G. Wolynes, J. Chem. Phys. **86**, 5133 (1987).
[30] A. Chandra and B. Bagchi, Chem. Phys. Lett. **151**, 47 (1988).
[31] B. Bagchi and A. Chandra, J. Chem. Phys. **91**, 2594 (1989).
[32] B. Bagchi and A. Chandra, Chem. Phys. Lett. **155**, 533 (1989).
[33] B. Bagchi, A. Chandra, and G. R. Fleming, J. Phys. Chem. **94**, 5197 (1990).
[34] Y. J. Yan, M. Sparpaglione, and S. Mukamel, J. Phys. Chem. **92**, 4842 (1988).
[35] M. Sparpaglione and S. Mukamel, J. Phys. Chem. **91**, 3938 (1987).
[36] Y. J. Yan and S. Mukamel, J. Phys. Chem. **93**, 6991 (1989).
[37] Y. J. Yan and S. Mukamel, J. Chem. Phys. **89**, 5160 (1988).
[38] M. Sparpaglione and S. Mukamel, J. Chem. Phys. **88**, 3263 (1988), and M. Sparpaglione and S. Mukamel, J. Chem. Phys. **88**, 4300 (1988).
[39] S. Mukamel and Y. J. Yan, Acc. Chem. Res. **22**, 301 (1989).
[40] Y. S. Bai and M. D. Fayer, Phys. Rev. B **39**, 11066 (1989).
[41] A. Garg, J. N. Onuchic, and V. Ambergaokar, J. Chem. Phys. **83**, 4491 (1985).
[42] J. N. Onuchic, D. N. Beratan, and J. J. Hopfield, J. Phys. Chem. **90**, 3707 (1986).
[43] J. N. Onuchic, J. Chem. Phys. **86**, 3925 (1987).
[44] J. N. Onuchic and D. N. Beratan, J. Phys. Chem. **92**, 4817 (1988).
[45] J. N. Onuchic and P. G. Wolynes, J. Phys. Chem. **92**, 6495 (1988).
[46] D. N. Beratan and J. N. Onuchic, J. Chem. Phys. **89**, 6195 (1988).
[47] L. D. Zusman, Chem. Phys. **49**, 295 (1980).
[48] L. D. Zusman, Chem. Phys. **119**, 51 (1988).
[49] I. Rips and J. Jortner, J. Chem. Phys. **87**, 2090, 6513 (1987).
[50] I. Rips and J. Jortner, J. Chem. Phys. **88**, 818 (1988).
[51] T. Fonseca, J. Chem. Phys. **91**, 2869 (1989).
[52] A. Blumen and J. Manz, J. Chem. Phys. **71**, 4694 (1979).
[53] A. Blumen, J. Chem. Phys. **74**, 6926 (1981).
[54] K. Allinger and A. Blumen, J. Chem. Phys. **72**, 4608 (1980) and K. Allinger and A. Blumen, J. Chem. Phys. **75**, 2762 (1981).
[55] H. Sumi and R. A. Marcus, J. Chem. Phys. **84**, 4894 (1986).
[56] Y. Lin, R. C. Dorfman, and M. D. Fayer, J. Chem. Phys. **90**, 159 (1989).
[57] R. C. Dorfman, Y. Lin, and M. D. Fayer, J. Phys. Chem. **93**, 6388 (1990).
[58] Y. Lin, R. C. Dorfman, and M. D. Fayer, J. Chem. Phys. **93**, 3550 (1990).
[59] S. Ojima, H. Miyasaka, and N. Mataga, J. Phys. Chem. **94**, 5834 (1990).
[60] J. Najbar, Chem. Phys. **131**, 325 (1989).
[61] J. Najbar and A. M. Turek, Chem. Phys. **142**, 35 (1990).
[62] H. Stehfest, Commun. ACM **13**, 47 (1970).
[63] W. H. Press, B. P. Flannery, S. A. Teukolsky, and W. T. Vetterling, *Numerical Recipes In C* (Cambridge University, Cambridge, 1988).
[64] R. C. Dorfman, Y. Lin, and M. D. Fayer, J. Phys. Chem. **94**, 8007 (1990).